Palladium nanoparticles supported on activated carbon (C) for the catalytic hexavalent chromium reduction

İbrahim Gözeten (ibrahim6349@hotmail.com)

Van Yüzüncü Yıl Üniversitesi Fen Fakültesi: Van Yuzuncu Yil Universitesi Fen Fakultesi

https://orcid.org/0000-0003-0346-9958

Mehmet Tunç

Van Yüzüncü Yıl University Institute of Natural and Applied Sciences: Van Yuzuncu Yil Universitesi Fen Bilimleri Enstitusu

Research Article

Keywords: Chromium, Formic Acid, Nanocatalyst, Palladium, Reduction, Kinetic

Posted Date: September 17th, 2021

DOI: https://doi.org/10.21203/rs.3.rs-887515/v1

Version of Record: A version of this preprint was published at Water, Air, & Soil Pollution on December 22nd, 2021. See the published version at https://doi.org/10.1007/s11270-021-05479-4.

Abstract

Hexavalent chromium is widely used in industry and causes human health and environmental problems due to its extremely toxic properties. On the contrary, trivalent chromium is necessary for living ecosystems. Therefore, it is best idea to detoxicate hexavalent chromium by reducing hexavalent chromium to trivalent chromium.. Pd(0)@C catalyst was prepared in solution under mild conditions by a simple impregnation-reduction method and was identified by XPS, XRD, TEM, TEM-EDX, HR-TEM, ICP-OES analyses. TEM results showed that very well dispersed Pd nanoparticles were formed on the C surface (mean particle sizes 3.98 ± 0.24 nm). The catalytic activity of Pd(0)NPs impregnated on C was tested in hexavalent chromium reduction in the reducing agent formic acid medium. The activated carbon supported Pd(0)@C nanoclusters were used as heterogeneous nanocatalysts in the catalytic reduction of Hexavalent chromium in formic acid medium, which is a good reducing agent under mild conditions. It was determined that the formed Pd(0) nanoclusters could successfully reduce Cr(VI) to Cr(III) by high selectivity (~ 97%). It was observed that the Pd(0)@C catalyst retained a significant (> 75%) initial activity even after the 5th use. In addition, for the kinetic data of the catalytic reduction reaction of Cr(VI) catalyzed by Pd(0)@C, the rate equation and activation parameters were derived depending on the $[Cr_2O_7^{2-}]$, [Pd(0)@C], [HCOONa], [HCOOH]concentrations and temperature.

Introduction

Cr(VI) has proven to be a mutagenic, acute toxicity carcinogen in its compounds (Elliott and Zhang 2001; Stearns et al. 1995). Chromium (VI) are used in various industrial areas (such as wood protection, metal plating, pigment production, corrosion inhibition, and electroplating) (Parabhakaran et al. 2009; Chen et al. 2013; Keith and Telliard 1979; Kotas and Stosicka 2000). Cr(VI)-containing industrial wastewater is considered as the second heavy metal pollutant (Yadav and Xu 2013). WHO (World Health Organization) stated that the level of hexavalent chromium in drinking water should be less than 0.05 mgL^{-1} (WHO 2008). Trivalent chromium on the other hand, less mobile in nature, is less toxic, and is an necessary nutrition for living things in trace amounts (Celebi et al. 2016; Zhitkovitch 2011; Kyung et al. 2005). Therefore, it is a good idea to detoxify hexavalent chromium by reducing it to trivalent chromium (Celebi et al. 2016). They tried various catalytic materials such as Fe(II) based minerals, bacterial strains, ZnO nanorods and sulphides in the reduction of Cr(VI) (Lan et al. 2005; Shirzad-Sibani et al. 2014; Hsu et al. 2010; Buerge and Hug 1998). Transition metal NPs have been in great demand recently due to their superior performance in the catalyzed reduction reaction of Cr(VI) (Barakat et al. 2013; Zahmakiran and Ozkar 2011). In particular, nanoclusters such as amino-functionalized palladium nanowires (Wei et al. 2015), PSA-saported palladium nanoparticles (Fu et al. 2014) and PVP- immobilized palladium nano-tetrapods showed high activity in reducing hexavalent chromium in the presence of reducing agent HCOOH (FA) (Omole et al. 2007). In FA catalytic decomposition CO_2 and H_2 ($HCOOH \rightarrow CO_2 + H_2$) are released (Yadav and Xu 2012; Yurderi et al. 2014). Then, the released H_2 is stabilized on the palladium nanoparticles and Cr(VI) is reduced to Cr(III) ($Cr_2O_7^{2-} + 8H^+ + 3H_2 \rightarrow 2Cr^{3+} + 7H_2O$) (Huang et al. 2012; Fu et al. 2014; Celebi et al. 2016). However, aggregation occurs in the active centers of collidal Pd

nanoparticles due to their multiple use, which reduces their activity (Fu et al. 2014; Wei et al. 2015; Omole et al. 2007). In order to prevent agglomeration on the surfaces of Pd nanocatalysts and to easily separate them from the solution, the idea of impregnating palledium nanoparticle onto the surface or inside of the support came to the fore. (Liang et al. 2013; Elliott and Zhang 2001; Dandapat and Jana 2011; Huang et al. 2012;Yang et al. 2010). Therefore, many different solid support materials are now preferred to stabilize guest palladium nanoparticles. Yadav et al. (Yadav and Xu 2013) stabilized Pd nanoparticles on MIL-101 metal-organic framework to isolate Cr(VI) from industrial wastewater. Huang and coworkers (Huang 2012) used Pd NPs as a reusable catalyzed material for the reduction reaction of Cr(VI) under mild conditions by impregnation on electrospun polymer nanofibers. Dandapat and coworkers (Dandapat and Jana 2011) used γ-Al_2O_3 films prepared after hydrolysis of peptization of Al(OOH) as support material for Pd NPs. Nanoparticles stabilized on suitable support materials prevent metal aggregation, reduce metal loading, increase electrochemical stability and activity, and prolong catalyst life (Wei et al. 2015; Yurderi et al. 2014). Therefore, it is i significant to develop new Pd NPs catalysts supported on suitable support material to increase the reduction reaction rate of hexavalent chromium (Celebi et al. 2016). In particular, carbon nanofibers, carbon derivatives containing carbon nanofibers, carbon black, graphite, carbon nanotubes, graphene and its derivatives are excellent support materials due to their excellent strength, superior stability and large surface areas (Demir et al. 2017). Therefore, we developed the previously unused Pd@C catalyst for the reduction reaction of Cr(VI) in FA medium.

Materials And Methods

Devices and materials

Sodium Formate (HCOONa), Formic Acid (HCOOH), $NiCl_2.6H_2O$, $RuCl_3.3H_2O$, $Pd(NO_3)_2{\cdot}2H_2O$ (~40% Pd), activated carbon(C), sodium borohydride ($NaBH_4$), sodium hydroxide (NaOH), potassium dichromate ($K_2Cr_2O_7$) and ethanol (C_2H_5OH) from Sigma-Aldrich received®. Nuve FN 300 oven (0-2500^{0}C), Heidolph MR-3004 magnetic stirrer, Lab Companion RW-0525 temperature bath, Shimadzu UV-2600 DR/UV-vis

Preparation of the catalysts (Pd@C, Ni@C, Ru@C)

Nanocatalysts were synthesized in a simple and reproducible manner by conventional impregnation and simultaneous reduction method of Pd, Ru and Ni metals on activated carbon (C) (Zhu and Xu 2015; Yang et al. 2010; Celebi et al. 2016).

a. Pd@C synthesis; Pd metal was supported on 100 mg C in 5.0 mg water ($Pd(NO_3)_2.2H_2O$ (4.95 mg, 19.20 µmol Pd) (mixed at 700 rpm for 2 hours)) and reduced with $NaBH_4$ (11.12 mg, 0.3 mM).
b. Ru@C synthesis; Ru metal was supported on 100 mg C in 5.0 mg water ($RuCl_3.3H_2O$ (5.28 mg, 20.18 µmol Ru) (mixed at 700 rpm for 2 hours)) and reduced with $NaBH_4$ (11.69 mg, 0.32 mM).
c. Ni@C synthesis; Ni metal was supported on 100 mg C in 5.0 mg water ($NiCl_2.6H_2O$ (8.32 mg, 35 µmol Ni) (mixed at 700 rpm for 2 hours)) and reduced with $NaBH_4$ (20.16 mg, 0.54 mM).

Then the mixtures were filtered and washed with plenty of water (3x10 mL), nanocatalysts were obtained in powder form, dried in a vacuum oven at 150 ^{0}C for 1 hour.

Catalytic experiments

$K_2Cr_2O_7$ (10 mL, 2.0 mM, 5.89 mg) solution was transferred to the reaction vessel, 10.0 mg of Pd(0)@C nanocatalyst was added, and the reaction equilibrated at 298 K for 15 minutes. Then, 1.0 mL solution (HCOONa; 312.3 mg, 450 M + HCOOH; 173.2 µL 0.45 M) was transferred to the reaction vessel with a 1.0 mL gas-insulated syringe. Immediately after, the catalyzed reaction was initiated with turning on the stirrer (> 700 rpm), at 0 min and then at certain time intervals, 0.9 mL of solution was taken from the sample cup, diluted to 1.0 mL with water, read in UV (Shimadzu UV-2600 spectrometer).

Identification of gaseous products from the decomposition of formic acid over Pd@C catalyst

Before beginning the catalytic reaction of FA, the hot water bath (Lab Companion RW-0525) was adjusted to a constant temperature of 25 ^{0}C, and a Schlenk type jacketed reaction vessel (50.0 mL) fixed onto a magnetic stirrer (Heidolph MR-3004). The Pd@C catalyst (10.0 mg) was transferred to the reaction vessel Schlenk, and 9.0 mL of H_2O was added to it, and thermal equilibrium was achieved after 15 minutes. Next, 1.0 mL of formic acid + sodium formate solution (450 mM FA + 450 mM SF) was transferred to the reaction vessel and the catalyzed reaction was initiated by operating the stirrer (> 700 rpm) (t = 0 minutes). The resulting gas was collected in the GC flask and analyzed with the Shimadzu TCD-2014 GC.

NaOH trap test

The trap test was carry out to determine the selectivity of the catalyst used in the catalytic decomposition reaction of FA. The trap experiment will give information about whether the reaction is proceeding through dehydrogenation or dehydration. Some researchers (Yadav et al. 2012; Celebi et al. 2016; Gu et al. 2011) have performed the NaOH trap experiment. The gas released from the dehydrogenation of FA is passed through a saturated NaOH (10.0 M) solution before the gas burette. When the reaction takes place with high selectivity, since all of the CO_2 gas formed together with the H_2 gas will react with NaOH in the trap, the gas volume to be measured should be halved ($2NaOH(aq) + CO_2(g) \rightarrow Na_2CO_3(aq) + H_2O(s)$).

UV/vis spectroscopic studies

The absorption peak of hexavalent chromium was measured with UV/vis spectroscopy at a fixed wavelength at 350 nm. Calculation of the concentration of remaining hexavalent chromium was made with a calibration curve obtained from the absorbance of standard solutions. The degree of catalytic reduction, also referred to as cycle, was calculated from the equation Conversion=[Cr(VI)]/$[Cr(V1)]_0$. Here, $[Cr(IV)]_0$ and [Cr(VI)] are the initial and specific time, respectively.

Confirmation of the presence of Cr(III) as a catalytic reaction product

Extra NaOH was transferred to the solution resulting from the conversion of hexavalent chromium, forming a green colored hexahydroxochromat(III) solution, confirming the formation of Cr(III) in solution (Zhu and Xu 2015; Yang et al. 2010; Celebi et al. 2016; Bulut et al. 2015).

Reusability performance

After the first catalytic cycle, the catalyst (Pd@C) was was purged from the solution medium, dried and used in the next cycle. The number of cycles was repeated up to 5.

Kinetic studies

Effects of sodium formate [HCOONa], formic acid [HCOOH], dichromate [$Cr_2O_7^{2-}$], catalyst [Pd(0)@C] concentrations and temperature on the catalytic reduction of Cr(VI) to Cr(III)

The effects of FA (0, 122.5, 225, 450, 675 mM), SF (0, 122.5, 225, 450, 675 mM), Dichromate (1.0, 2.0, 4.0, 8.0 mM), catalyst (5.0, 7.5, 10.0, 15.0 mg Pd(0)@C, 1.37% by weight Pd loadings correspond to 0.065, 0.098, 0.129, 0.196 mM Pd) initial concentrations and temperature (298-318 K) onto the catalytic reduction of Cr(VI) to trivalent chromium were investigated.

The superiority of Pd@Ccatalyst

To determine the superiority of Pd(0)@C catalyst over Ru(0)@C and Ni(0)@C nanocatalysts, The reduction of Cr(VI) was investigated in the same test standards (10.0 mL water; 312.3 mg, 450 mM HCOONa; 173.2 µL, 450 mM HCOOH; 2.0 mM, 5.89 mg $K_2Cr_2O_7$) and 298 K.

Results And Discussion

Characterization of Pd NPs stabilized on activated carbon (C)

The nature of the prepared Pd@C nanoclusters was described using P-XRD, ICP-OES, DR/UV-vis, TEM-EDX, HRTEM, XPS techniques. The Pd ratio in the Pd(0)@C' catalyst was determined by ICP-OES (1.37 wt% Pd) (Yang et al. 2010; Celebi et al. 2016; Liang et al. 2013; Zhu and Xu 2015). Figure 2 presents the P-XRD patterns of C and Pd@C. When the Pd(0)@C and C peaks are examined carefully, it is seen that there is a decrease from the Pd(0)@C peaks compared to the C peaks (Fig. 1). The decrease in the specific BET surface was determined as 300 m^2/g for C and 250 m^2/g for Pd(0)@C. This decrease in the BET surface of Pd(0)@C indicates that Pd NPs are supported on C. It is seen that it gives diffraction peaks at 39.6^0, 46.5^0 and 67.8^0 degrees on the 111, 200 and 220 surfaces of Pd, respectively (JCPDS No. 05-0681) (JCPDS 1991) (Fig. 1). XPS analyzes were performed to define the oxidation steps of the Pd metal in the sample (Fig. 2). Signals were observed for $Pd^0 3d_{5/2}$ and $Pd^0 3d_{3/2}$ at binding energies of 334.5 and 339.8 eV, respectively (Fig. 2) (Yang et al. 2010; Celebi et al. 2016; Zhu and Xu 2015; Zhang et al. 2013; Abass 2005). TEM, TEM-EDX and HRTEM analysis techniques were used to describe the average particle size,

crystal structure and morphology of the activated carbon stabilized Pd(0)@C catalytic material. The presence of well-dispersed palladium NPs onto the C surface was revealed by TEM (Fig. 3a). The histogram showing the palladium NPs size ranging from 2.06 to 5.3 nm and the average palladium NPs size of 3.98 nm (Fig. 3(b)). The TEM-EDX spectrum shows the existence of Pd, O, C atoms in the sample Fig. 3 (c). The HRTEM image shows that the Pd nanoclusters formed in high crystallinity (Fig. 3d). The Pd fringe spacing was determined as 0.223 nm and 0.139 on the Pd(111) and Pd(200) surfaces, respectively (Schlotterbeck et al. 2014; Yang et al. 2014; Celebi et al. 2016; Zhang et al. 2013; Su et al. 2015; Zhu and Xu 2015).

Control experiments for the Pd(0)@C catalyzed decomposition reaction of formic acid

As in many studies, sodium formate was used as a trigger for the catalytic degradation reaction of FA (Yadav and Xu 2012; Wei et al. 2015; Celebi et al. 2016; Yurderi et al. 2014; Gu et al. 2011). Recent reports suggest that some homogeneous (Su et al. 2015; Kim et al. 2014) and heterogeneous (Celebi et al. 2016; Yang et al. 2010) catalysts may obtain H_2 not only from formic acid, but also from catalyzed hydrolysis of sodium formate ($HCOONa + H_2O \rightarrow H_2 + NaHCO_3$). To determine whether the resulting gas is from FA or SF, it must be confirmed by a control test. In the control experiment, we found that hydrolysis of SF released only 2.2 mL of H_2 gas even at 230 minutes at 318 K. It is significant to determine whether the Cr(VI) catalytic reduction reaction proceeds in the dehydrogenation ($HCOOH \rightarrow CO_2 + H_2$) pathway of FA or in the dehydration ($HCOOH \rightarrow H_2O + CO$) pathway (Zahmakiran et al. 2012; Enthaler et al. 2010). Because in trivalent chromium catalytic reduction, both H_2 (Celebi et al. 2016; Roucoux et al. 2002) and CO (Cannors 1990) can act as reducing agents. Therefore, NaOH trap test and GC/TCD analysis were carried out to define the selectivity of Pd(0)@C nanocatalyst in the degradation reaction of FA (Liang et al. 2013; Celebi et al. 2016; Yurderi et al. 2014; Gu et al. 2011; Yadav and Xu 2012). At the end of the NaOH trap, it was seen that the total volume of gas produced was halved (Fig. S1).

Monitoring of catalytic reduction reaction and reactivity of catalytic palladium-free C

The effect onto the catalytic performance of nanocatalyst (Pd(0)@C) onto the reaction rate in the reduction reduction of Cr(VI) was determined with many experiments. $K_2Cr_2O_7$ was preferred as the hexavalent chromium source. The characteristic peak of Cr(VI) due to the charge transfer transition (LMCT) from ligand (oxygen) to metal (Cr(VI)) was measured at 350 nm at a fixed wavelength (Wei et al. 2015; Liang et al. 2013; Yang et al. 2010; Yurderi et al. 2014; Celebi et al. 2016; Yadav and Xu 2012; Gu et al. 2011). This makes it possible to study the reduction processes of Cr(VI) with UV/vis. Before starting testing the activity of the Pd(0)@C catalytic material, the catalytic activity of the activated carbon support material was tested. It was observed that the characteristic peak at 350 nm remained constant for 70 min without loading Pd NPs. It was observed that the absorption peak at 350 nm remained unchanged for 70 min without Pd NPs (Fig. 4 (a)). This indicates that reduction cannot occur without Pd NPs. When a very

small amount of Pd NPs (10.0 mg Pd(0)@C, 1.29 µmol Pd) was loaded onto the C solid support, the characteristic absorption peak at 350 nm completely reduced at 65 min (Fig. 4 (b)). Initially yellow, the potassium dichromate solution turned into a colorless solution after completing the catalytic cycle. The presence of Cr(III) was confirmed with transferring NaOH to this colorless solution. It was observed that the color of the colorless solution turned green with NaOH transfer. This shows the formation of hexahydroxochrome(III) ($[Cr(OH)6]^{-3}$), which is evidence of the presence of Cr(III). The pH of the catalytic reduction was also observed. It was found that the pH of the solution was 3.58 at the beginning, then increased to 3.62 and remained stable at this value until the catalytic cycle was completed.

Uniqueness of Pd(0)@C in the catalytic reduction of Cr(VI) to Cr(III)

In this study, easily available and inexpensive C was preferred as solid support material. In the catalytic reaction, the superiority of Pd metal was investigated by comparing it with Ru and Ni metals The catalytic activities of Pd(0)@C, Ru(0)@C and Ni(0)@C nanocatalysts in Cr(VI) reduction were tested. With Ru (10.0 mg; 1.37% Ru, 1.36 µmol Ru) and Ni (10.0 mg; 1.40% Ni, 2.38 µmol Ni) metal loading, the characteristic peak of Cr(VI) at 350 nm remained constant up to 70 min (Fig. S2 and S3), on the contrary, Pd metal loading (10.0 mg; 1.37% Pd, 1.29 µmol Pd) was completely reduced in 65 minutes (Fig. S4). This indicates that the activity of palladium nanoparticles is higher for this reaction.

Catalytic stability of Pd@C in the catalytic reduction of Cr(VI)

The stability of the Pd(0)@C nanocatalyst was tested in the reduction of Cr(VI) for purification from solution and reusability. After the 1st catalytic cycle is complete (Fig. 5(a)), the catalyst was removed from the solution medium and used in the next conversion. The number of catalytic conversions was repeated as 5, and it was found that it retained > 75% of its initial activity even after the 5th catalytic conversion (Fig. 5(b)). The TEM image of the 5th catalytic cycle is given in Fig. 5(c) and the average particle size obtained from this TEM image was determined as 5.30 nm (Fig. 5(d)). The average Pd NPs size appears to have increased from 3.98 ± 0.24 nm (fresh) to 5.30 ± 0.21 nm (at the end of the 5th conversion), hence a slight increase in particle size. This increase indicates a decrease in the activity of the nanocatalyst. In addition, Pd metal was not found in the 5th catalytic cycle ICP-OES analysis, indicating that Pd nanoclusters were supported on the C support material without leaking into the solution.

Kinetic studies

To the catalyzed reduction reduction hexavalent chromium, kinetic studies were first initiated by attempts to determine the most effective ratios of (Fig. S5) and [SF] (Fig. S6) concentrations. Figure 6 (a and c) shows the remaining of Cr(VI) fraction to initial concentration ($[Cr(VI]/[Cr(VI)]_0]$) against time. It was determined that Cr(VI) was not reduced to Cr(III) when FA was not added to the catalytic reaction, but

gradually reduced when SF was not added, adding FA up to 0.45 M increased the reaction rate, but did not increase the reaction rate at further concentrations (as in reaction kinetics) (Zahmakiran and Ozkar 2006; Celebi et al. 2016) (Fig. 6 (b)). It was observed that increasing the concentration of SF up to 0.45 M played a triggering (p) role onto the reduction rate of Cr(VI) to Cr(III), but adding more than 0.45 M decreased the reduction rate (Fig. 6(d)). The reason for thismay can be explained with the formate anion poisoning the surfaces of the active Pd centers (Durap et al; 2009; Zahmakiran and Ozkar 2006). Therefore, in this study, FA/SF concentrations were kept constant at 0.45 M/0.45 M, which is the most effective ratio. The graph of the Cr(VI) fraction remaining in solution ($[Cr(VI]/[Cr(VI)]_0$] against time, created with diverse Pd concentrations (Fig. S7), is given in Fig. 7(a) Observed rate constants (k_{obs}) obtained from the linear sections of the graph in Fig. 7(a). The graph of the $\ln k_{obs}$ against ln[Pd] is given in Fig. 7(b)). According to the 1.39 slope of Fig. 7(b), the catalytic reduction takes place in the first order depending on the concentration of Pd. The ratio of Cr(VI) remaining in solution ([Cr(VI]/[Cr(VI)]0]) against time, generated from diverse initial concentrations of Cr_2O_7 (Figure S8), is given in Fig. 7(c). $\ln k_{obs}$ against the $\ln[Cr_2O_7^{2-}]$ substrate concentration is given in Fig. 7(d). Considering the slope of this graph, it is seen that the catalytic reduction takes place by a slope of 0.23 degrees depending on the dichromate concentration.

In addition, the effect of temperature as well as substrate and palladium nanoparticles concentrations onto the reduction rate of the catalyzed reaction was investigated. The effect of temperature onto the reduction rate of Cr(VI) has been investigated in many experiments at different temperatures (298–318 K) (Fig. S9). UV-Vis spectroscopy of Cr(VI) catalytic conversion at 298, 303, 308, 313 and 318 K at t = 1 min is given in Fig. 8 (a). It seems that the reduction ratio of Cr(VI) increases as the temperature increases. Figure 8 (b) indicates the graph of the fraction of Cr(VI) remaining in solution ([Cr(VI]/[Cr(VI)]0]) against time, obtained at different temperature range (298-318K). The activity values of Pd(0)@C catalyst at 298, 303, 308, 313 and 318 K temperatures, respectively; 31, 33, 36, 47, 57 mol $Cr_2O_7^{2-}$/mol Pd min. was determined as. These activity values are higher than the activity values of PdNPs@polymer-nanofibers (at 323 K, 2.32 mol $Cr_2O_7^{2-}$/mol Pd min) (Huang et ak. 2012), palladium tetrapods (at 323 K, 4.23 mol $Cr_2O_7^{2-}$/mol Pd min) (Fu et al. 2014; Celebi et al. 2016) and supported Pd/PtNPs (at 318 K, 1.66 mol $Cr_2O_7^{2-}$/mol Pd min) (Liang et al. 2014). Arrhenius graph (Fig. 8 (c)) and Eyring-Polanyi graph (Fig. 8(d)) were drawn from the k_{obs} calculated from the graphs of five different temperatures (Fig. 8 (b)). Then, the activation parameters Ea from the Arrhenius graph, $\Delta Ha^{\neq}$ and $\Delta Sa^{\neq}$ from the Eyring-Polanyi graph were calculated. The activation values of Ea, $\Delta Ha^{\neq}$, $\Delta Sa^{\neq}$ for Pd(0)@C are respectively; It was calculated as 39.0 kJ/mol, 53.4 kJ/mol and − 210.0 J/mol K. The activation enthalpy (39.0 kJ/mol) obtained from the reduction of Cr(VI) with Pd(0)@C is lower than that obtained in the existence of Pd@□□-$A1_20_3$ catalyst (76.2 kJ/mol) (Yang et al. 2010; Dandapat and Jana 2011; Huang et al. 2012; Celebi et al. 2016). The low positive activation enthalpy and negative activation entropy shows that the reduction of Cr(VI) with Pd(0)@C catalyst occurs by a transitional associative mechanism.

Conclusions

In summary, Pd^{2+} particles were supported on activated carbon in solution, followed by reduction to Pd(0) with NaBH4 under mild conditions, to synthesize the Pd(0)@C nanocatalyst in a simple and reproducible manner. Then characterization was performed by P-XRD, ICP-OES, HRTEM, DR/UV-vis, TEM-EDX, XPS. The results of the analysis showed that very well dispersed palladium nanoparticle (average particle size 3.98 nm) were formed on the activated carbon. The durability, catalytic performance and activity of the Pd(0)@C nanocatalyst were investigated in the catalytic reduction of Cr(VI) to Cr(III) in FA medium as reducing agent at 298 K. The Pd(0)@C catalyst showed to be a heterogeneous nanocatalyst with usable activity (TOF = 31 mol $Cr_2O_7^{2-}$/mol Pd min) in the catalytic reaction. Moreover, the first synthesized Pd(0)@C nanocatalyst proved to have outstanding resistance to solution seepage and aggregation, retaining > 75% of its initial activity even after the 5th catalytic cycle. As a result, we believe that the Pd(0)@C catalyst will lead to the synthesis of new catalysts.

Declarations

Acknowledgements

This study was supported by the Van Yüzüüncü Yıl University Scientific Research Projects Coordination Unit as a project numbered FDK-2019-8195.

The authors would like to thank the Scientific Research Projects Coordination Unit of Van Yüzüüncü Yıl University for their financial support.

Conflict of interest

The authors declare no competing interest

References

1. Abass E, Alireza M, Reza V (2005) Chromium (III) Removal and Recovery from Tannery Wastewater by Precipitation Process. Am J Appl Sci 2(10):1471. https://doi:10.3844/ajassp.2005.1471.1473
2. Barakat T, Rooke JC, Genty E, Cousin R, Siffert S, Su BL (2013) Gold catalysts in environmental remediation and water-gas shift technologies. Energy Environ Sci 6(2):371–391
3. Buerge IJ, Hug SJ (1998) Influence of Organic Ligands on Chromium(VI) Reduction by Iron(II). Environ Sci Technol 32(14): 2092–2099. https:// doi.org/10.1021/es970932b
4. Bulut A, Yurderi M, Karatas Y, Zahmakiran M, Kivrak H, Gulcan M, Kaya M (2015) Pd-MnO_x nanoparticles dispersed on amine-grafted silica: Highly efficient nanocatalyst for hydrogen production from additive-free dehydrogenation of formic acid under mild conditions. App Catal B: Environ 164:324–333. https://doi.org/10.1016/j.apcatb.2014.09.041
5. Celebi M, Yurderi M, Bulut A, Kaya M, Zahmakiran M (2016) Palladium nanoparticles supported on amine-functionalized SiO2 for the catalytic hexavalent chromium reduction. Appl Catal B 180:53–64. https://doi.org/10.1016/j.apcatb.2015.06.020

6. Chen JH, Hsu KC, Chang YM (2013) Surface modification of hydrophobic resin with tricaprylmethylammonium chloride for the removal of trace hexavalent chromium. Ind Eng Chem Res 52(33):11685–11694. https://doi.org/10.1021/ie401233r
7. Connors KA (1990) Theory of Chemical Kinetics. VCH Publishers, New York
8. Dandapat A, Jana D, De G (2011) Pd nanoparticles supported mesoporous γ-C film as a reusable catalyst for reduction of toxic Cr VI to Cr III in aqueous solution. Appl Catal A 396(1–2):34–39. https://doi:10.1016/j.apcata.2011.01.032
9. Demir E, Sen B, Sen F (2017) Highly efficient Pt nanoparticles and f-MWCNT nanocomposites based counter electrodes for dye-sensitized solar cells. Nano-Structures Nano-Objects 11:39–45. https://doi.org/10.1016/j.nanoso.2017.06.003
10. Durap F, Zahmakiran M, Ozkar S (2009) Water soluble laurate-stabilized rhodium(0) nanoclusters catalyst with unprecedented catalytic lifetime in the hydrolytic dehydrogenation of ammonia-borane. App Catal A: Gen 369(1–2):53–59. https://doi.org/10.1016/j.apcata.2009.08.031
11. Elliott DW, Zhang W (2001) Field assessment of nanoscale bimetallic particles for groundwater treatment. Environ Sci Technol 35(24):4922–4926. doi 10.1021/es0108584.
12. Enthaler S, Langermann JV, Schmidt T (2010) Carbon dioxide and formic acid—the couple for environmental-friendly hydrogenstorage? Energy Environ Sci 3:1207–1217
13. Fu GT, Jiang X, Wu R, Wei SH, Sun DM, Tang YW, Lu TH, Chen Y (2014) Arginine-Assisted Synthesis and Catalytic Properties of Single-Crystalline Palladium Tetrapods. ACS Appl Mater Inter 6(24):22790–22795. https://doi.org/10.1021/am506965f
14. Gu X, Lu Z-H, Jiang H-L, Akita T, Xu Q (2011) Synergistic catalysis of metal-organic framework-immobilized Au-Pd nanoparticles in dehydrogenation of formic acid for chemical hydrogen storage. J Am Chem Soc 13(31):1822–11825. doi 10.1021/ja200122f.
15. Hsu LC, Wang SL, Lin YC, Wang MK, Chiang PN, Liu JC, Kuan WH, Chen CC, Tzou YM (2010) Cr(VI) Removal on Fungal Biomass of *Neurospora crassa*: the Importance of Dissolved Organic Carbons Derived from the Biomass to Cr(VI) Reduction. Environ Sci Technol 44(16):6202–6208. https://doi.org/10.1021/es1017015
16. Huang Y, Ma H, Wang S, Shen M, Guo R, Cao X, Zhu M, Shi X (2012) Efficient catalytic reduction of hexavalent chromium using palladium nanoparticle-immobilized electrospun polymer nanofibers. ACS ApplMater Inter 4(6):3054–3061. https://doi:10.1021/am300417s
17. Joint Committee on Powder Diffraction Standards (1991), JCPDS International Center for Diffraction Data, Pennsylvania
18. Keith LH, Telliard WA (1979) ES&T Special Report: Priority pollutants: I-a perspective view. EnvironSci Technol 13(4):416–423. https:// doi.org/10.1021/es60152a601
19. Kim SM, Lee YJ, Kim JW, Lee SY (2014) Facile synthesis of Pt–Pd bimetallic nanoparticles by plasma discharge in liquid and their electrocatalytic activity toward methanol oxidation in alkaline media. Thin Solid Films 572:260–265. https://doi.org/10.1016/j.tsf.2014.07.067

20. Kotas J, Stasicka Z (2000) Chromium occurrence in the environment and methods of its speciation. Environ Pollut 107(3):263–283. doi:10.1016/s0269-7491(99)00168-2. https://
21. Kyung H, Lee J, Choi W (2005) Simultaneous and synergistic conversion of dyes and heavy metal ions in aqueous TiO_2 suspensions under visible-light ıllumination. Environ Sci Technol 39(7):2376–2382. https://doi.org/10.1021/es0492788
22. Lan Y, Deng B, Kim C, Thornton EC, Xu H (2005) Redox Interactions of Cr(VI) and Substituted Phenols: Kinetic Investigation. Environ Sci Technol 39(7):2087–2094. https://doi.org/10.1021/es00061a026
23. Liang M, Su R, Qi W, Zhang Y, Huang R, Yu Y, Wang L, He Z (2014) Reduction of Hexavalent Chromium Using Recyclable Pt/Pd Nanoparticles Immobilized on Procyanidin-Grafted Eggshell Membrane. Ind Eng Chem Res 53(35):13635–13643. https://doi.org/10.1021/ie5021552
24. Liang M, Wang L, Liu X, Qi W, Su R, Huang R, Yu Y, He Z (2013) Cross-linked lysozyme crystal templated synthesis of Au nanoparticles as high-performance recyclable catalysts. Nanotechnology 24:245601
25. Omole MA, K'Owino IO, Sadik OA (2007) Palladium nanoparticles for catalytic reduction of Cr(VI) using formic acid. Appl Catal B 76(1–2):158–167. https://doi.org/10.1016/j.apcatb.2007.05.018
26. Prabhakaran SK, Vijayaraghavan K, Balasubramanian R (2009) Removal of Cr(VI) Ions by Spent Tea and Coffee Dusts: Reduction to Cr(III) and Biosorption Ind. Eng Chem Res 48(4):2113–2117. https://doi.org/10.1021/ie801380h
27. Roucoux A, Schulz J, Patin H (2002) Aminopropyltriethoxysilane stabilized ruthenium(0) nanoclusters as an isolable and reusable heterogeneous catalyst for the dehydrogenation of dimethylamine-borane. Chem Rev 102(10):3757–3778
28. Schlotterbeck U, Aymonier C, Thomann R, Hofmeister H, Tromp M, Richtering W, Mecking S (2014) Document details - Shape-selective synthesis of palladium nanoparticles stabilized by highly branched amphiphilic polymers. Adv Func Mater 14(10):999–1004
29. Shirzad-Siboni M, Farrokhi M, Soltani RDC, Khataee A, Tajassosi S (2014) Photocatalytic reduction of hexavalent chromium over ZnO nanorods immobilized on Kaolin. Ind Eng Chem Res 53(3):1079–1087. https:// doi.org/10.1021/ie4032583
30. Stearns DM, Kennedy LJ, Courtney KD, Giangrande P, Phieffer LS, Wetterhahn KE (1995) Reduction of chromium(VI) by ascorbate leads to chromium-DNA binding and DNA strand breaks in vitro. Biochemistry 34(3):910–919. https://doi:10.1021/bi00003a025
31. Su N, Chen X, Ren Y, Yue B, Wang H, Cai W, He H (2015) The facile synthesis of single crystalline palladium arrow-headed tripods and their application in formic acid electro-oxidation. Chem Commun 51:7195–7198
32. Wei LL, Gu R, Lee JM (2015) Highly efficient reduction of hexavalent chromium on amino-functionalized palladium nanowires. App Catal B: Environ 176:325–330. https://doi.org/10.1016/j.apcatb.2015.03.056
33. World Health Organization (2008) Guidelines for Drinking Water Quality. WHO, Press, Geneva

34. Yadav M, Singh AK, Tsumori N, Xu Q (2012) Palladium silica nanosphere-catalyzed decomposition of formic acid for chemical hydrogen storage. J Mater Chem 22:19146–19150
35. Yadav M, Xu Q (2012) Liquid-phase chemical hydrogen storage materials. Energy Environ Sci 5:9698–9725
36. Yadav M, Xu Q (2013) Catalytic chromium reduction using formic acid and metal nanoparticles immobilized in a metal–organic framework. Chemicial Commun 49:3327–3329
37. Yang C, Manocchi AK, Lee B, Yi H (2010) Viral templated palladium nanocatalysts for dichromate reduction. App Catal B: Environ 93(3–4):282–291. https://doi.org/10.1016/j.apcatb.2009.10.001
38. Yang S, Shen C, Tian Y, Zhang X, Gao H-J (2014) Synthesis of cubic and spherical Pd nanoparticles on graphene and their electrocatalytic performance in the oxidation of formic acid. Nanoscale 6:13154–13162
39. Yurderi M, Bulut A, Zahmakiran M, Kaya M (2014) Carbon supported trimetallic PdNiAg nanoparticles as highly active, selective and reusable catalyst in the formic acid decomposition. App Catal B: Environ 160:514–524. https://doi.org/10.1016/j.apcatb.2014.06.004
40. Zahmakiran M, Leshkov YR, Zhang Y (2012) Rhodium(0) Nanoparticles Supported on Nanocrystalline Hydroxyapatite: Highly Effective Catalytic System for the Solvent-Free Hydrogenation of Aromatics at. Room TemperatureLangmuir 28(1):60–64. https://doi.org/10.1021/la2044174
41. Zahmakiran M, Ozkar S (2006) Water dispersible acetate stabilized ruthenium(0) nanoclusters as catalyst for hydrogen generation from the hydrolysis of sodium borohyride. J Mol Catal A: Chem 258(1–2):95–103. https://doi.org/10.1016/j.molcata.2006.05.037
42. Zahmakiran M, Ozkar S (2011) Metal nanoparticles in liquid phase catalysis; from recent advances to future goals. Nanoscale 3:3462–3481
43. Zhang Y, Gao H, Kuai Y, Han Y, Wang J, Sun B, Gu S, You W (2013) Effects of Y additions on the precipitation and recrystallization of Al-Zr alloys. Sci Rep 86:1–8. https://doi.org/10.1016/j.matchar.2013.09.004
44. Zhitkovich A (2011) Chromium in drinking water: Sources, metabolism, and cancer risks. Chem Res Toxicol 24(10):1617–1629. https://doi.org/10.1021/tx200251t
45. Zhu Q-L, Xu Q (2015) Liquid organic and inorganic chemical hydrides for high-capacity hydrogen storage. Energ Environ Sci 8:478–512. https://doi.org/10.1039/C4EE03690E

Figures

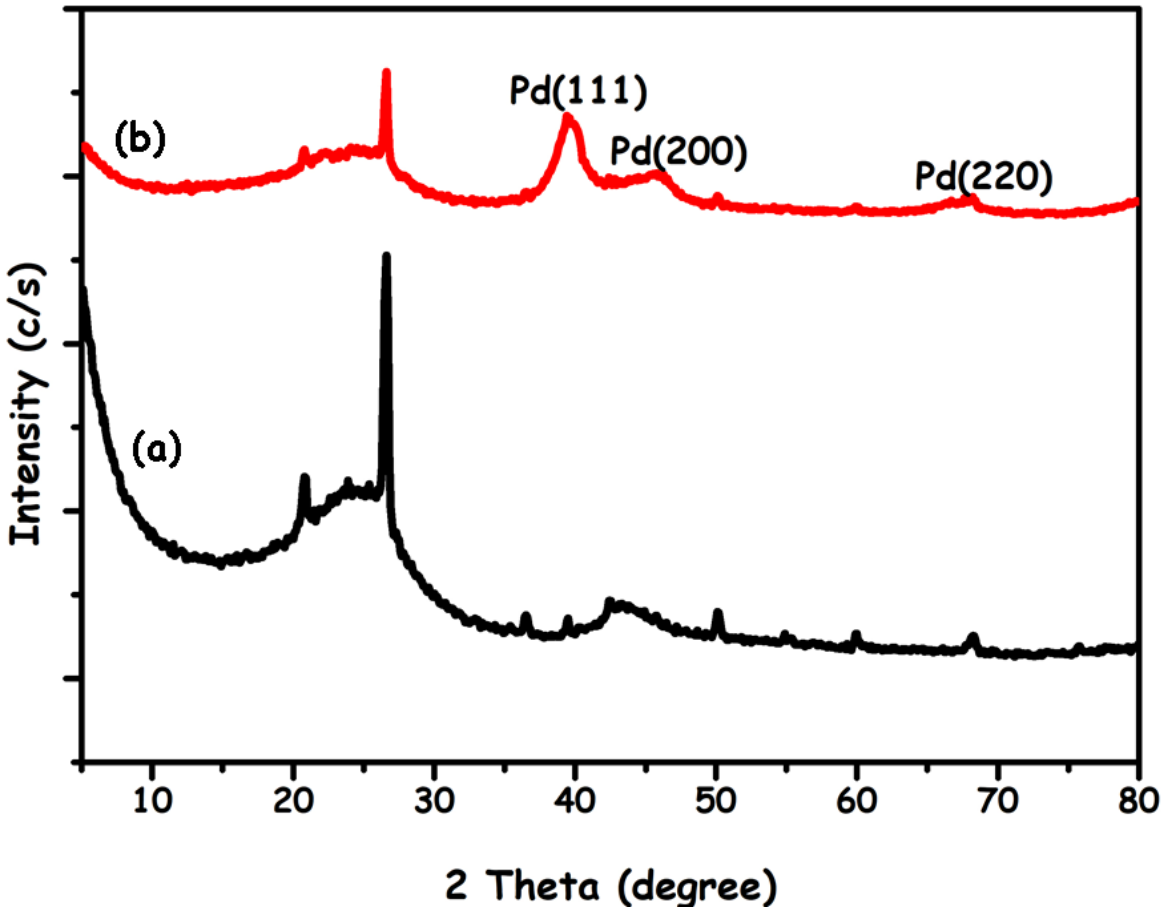

Figure 1

(a) C, (b) Pd(0)@C patterns of P-XRD in the 2θ = 10-800 range.

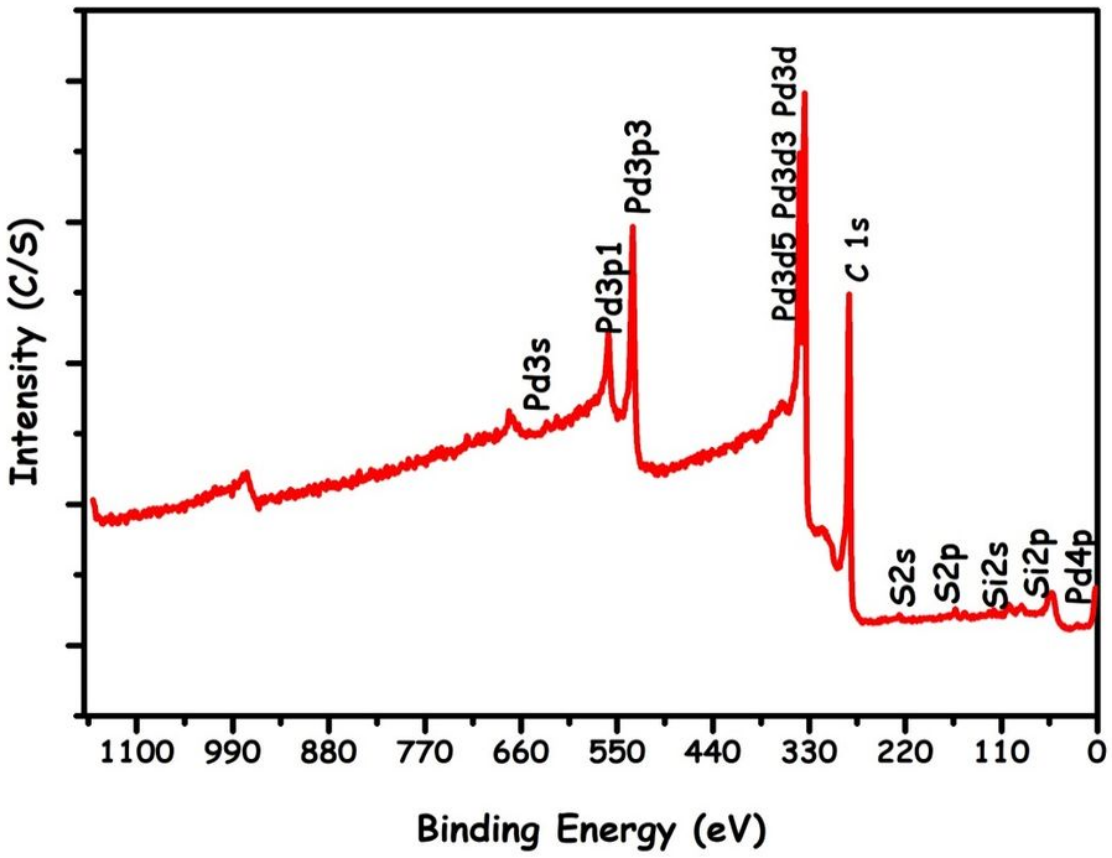

Figure 2

XPS of Pd(0)@C the survey spectrum.

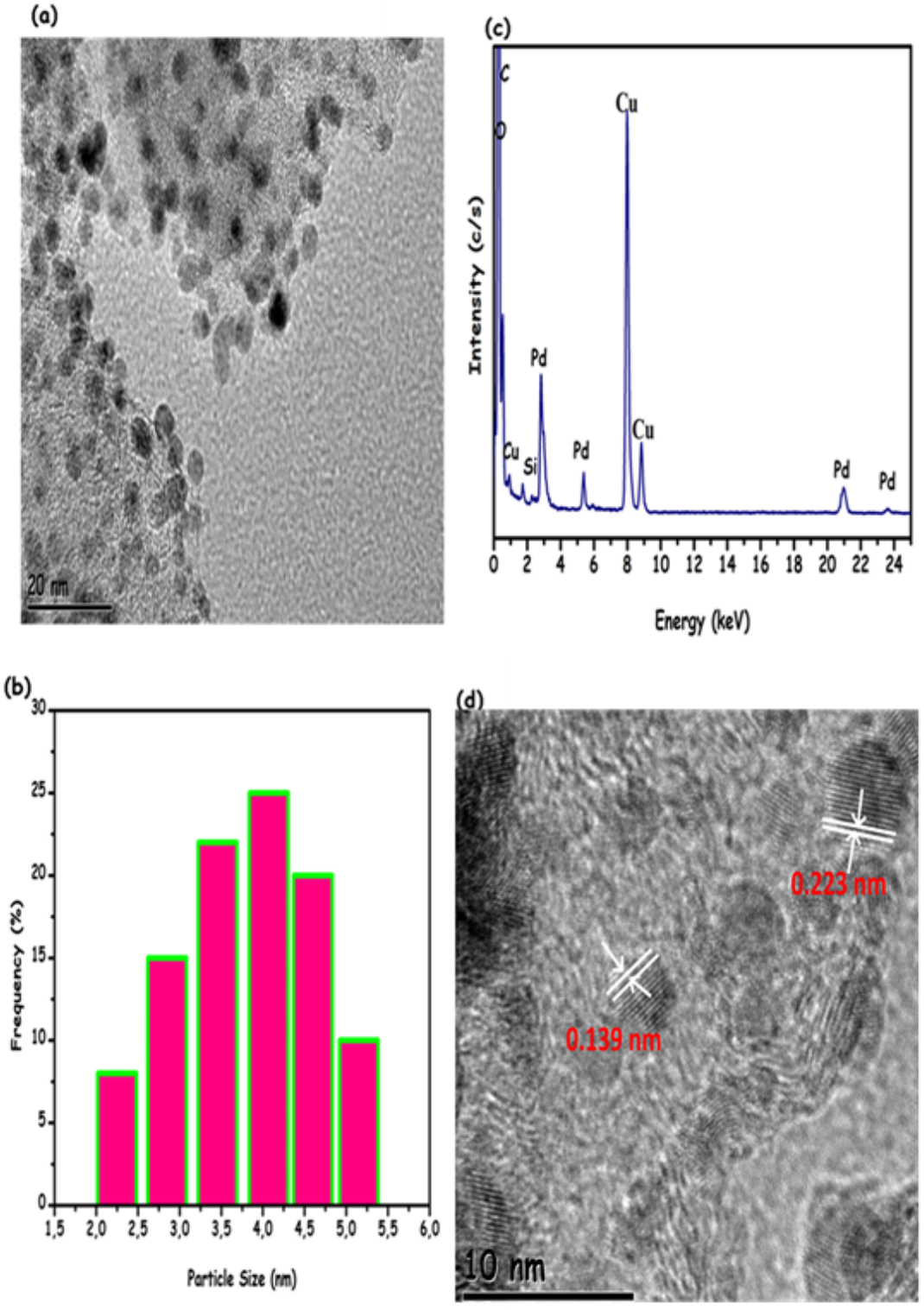

Figure 3

Pd(0)@C catalyst of (a) TEM image, (b) size histogram obtained from (d), (c) spectrum of TEM-EDX, (d) HRTEM image.

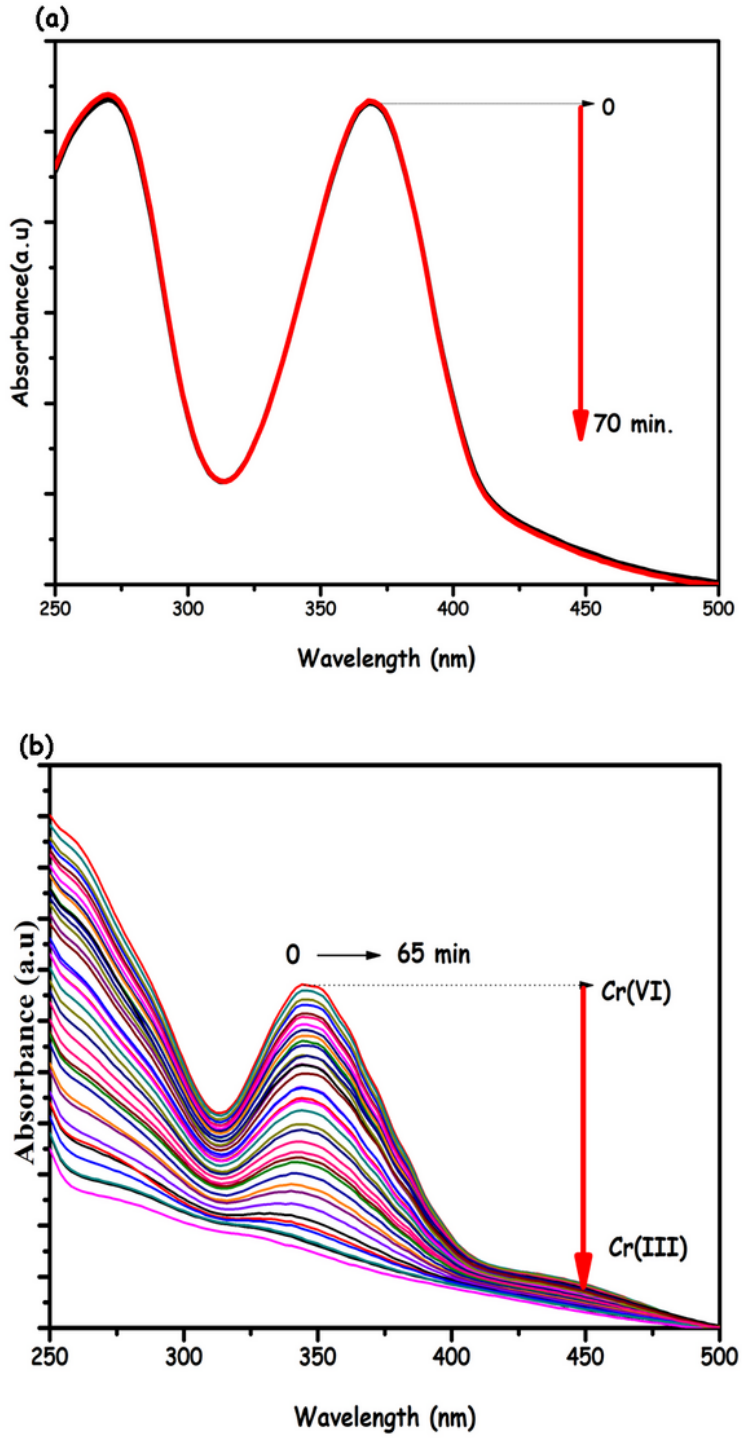

Figure 4

(a) 10 mg C, (b) 10 mg Pd(0)@C catalyst (containing 1.37% Pd; 0.129 mM Pd) at 298K.

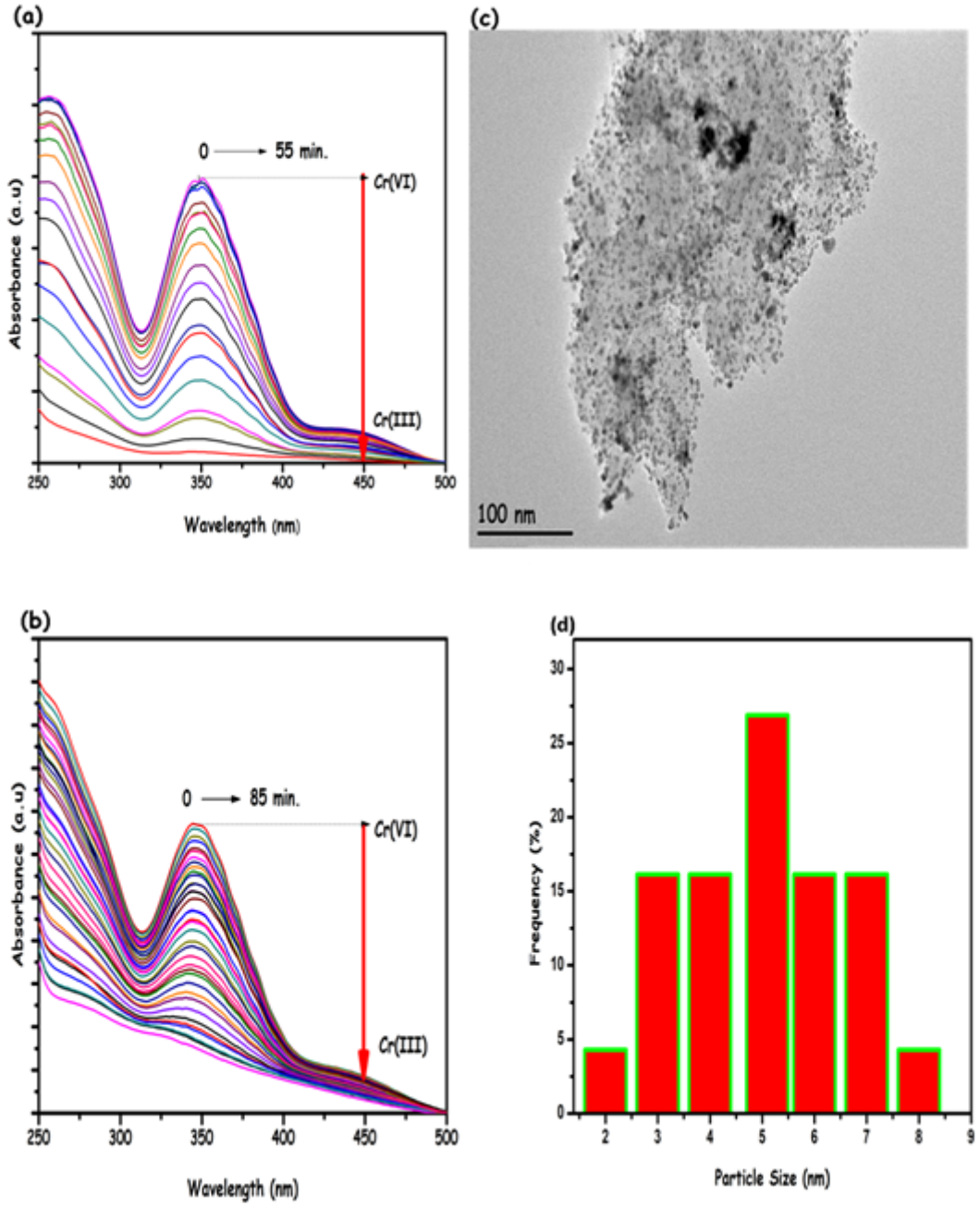

Figure 5

(a) 15 mg the Pd(0)@C catalyst (1.37 wt%, 193 mM Pd) 1st cycle, (b) 9.0 mg Pd(0)@C catalyst (1.37 wt %, 116 mM Pd) 5st cycle, (c) the TEM image of after 5th reuse, (d) is the size histogram obtained from (c).

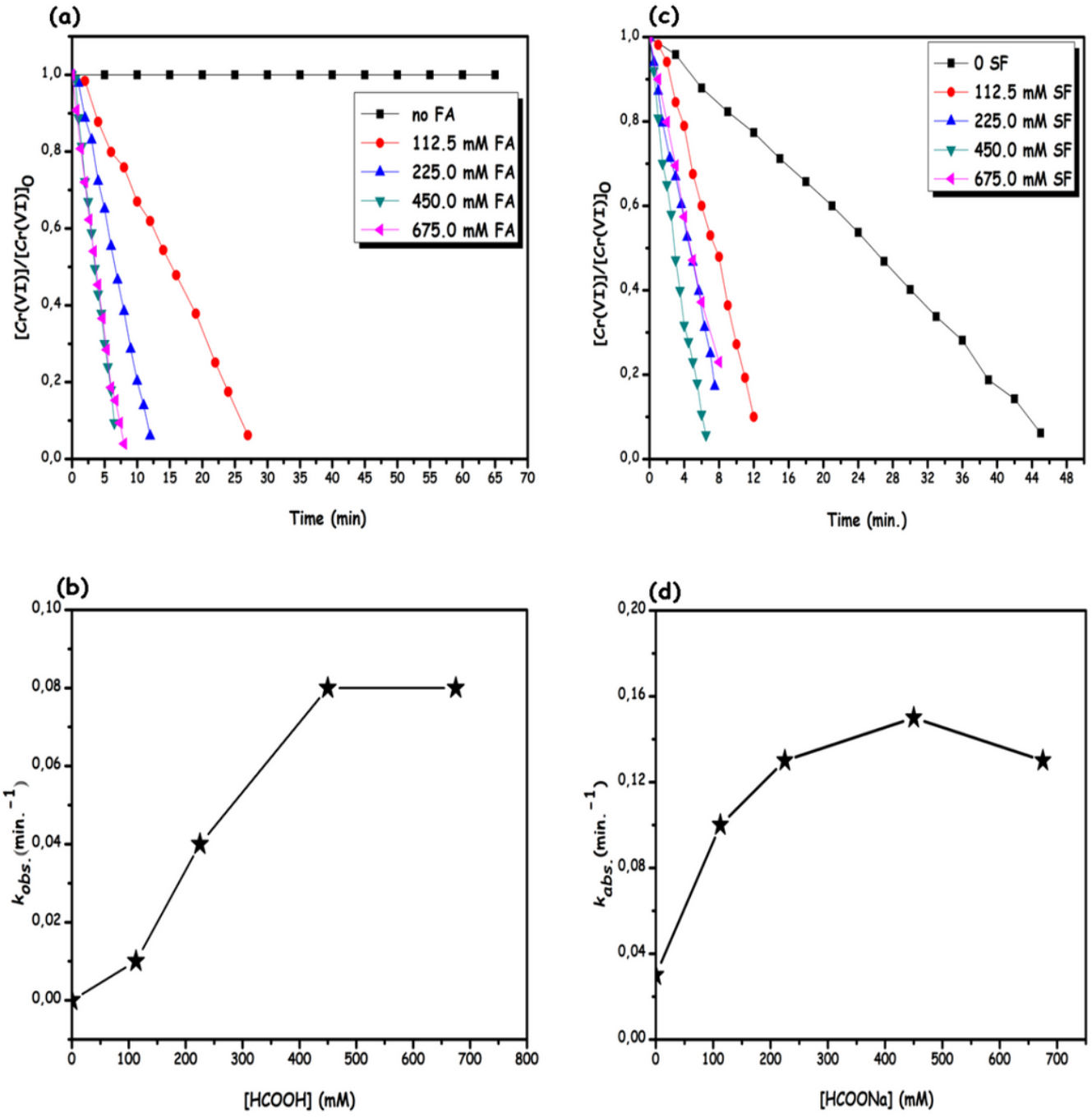

Figure 6

(a) Graph of remaining Cr(VI) ratio ([Cr(VI]/[Cr(VI)]0] against time, (b) graph of [HCOOH] concentration against kobs values obtained from (a), (c) graph of remaining Cr(VI) ratio ([Cr(VI]/[Cr(VI)]0] against time, (d) graph of [HCOONa] concentration against kobs values obtained from (c).

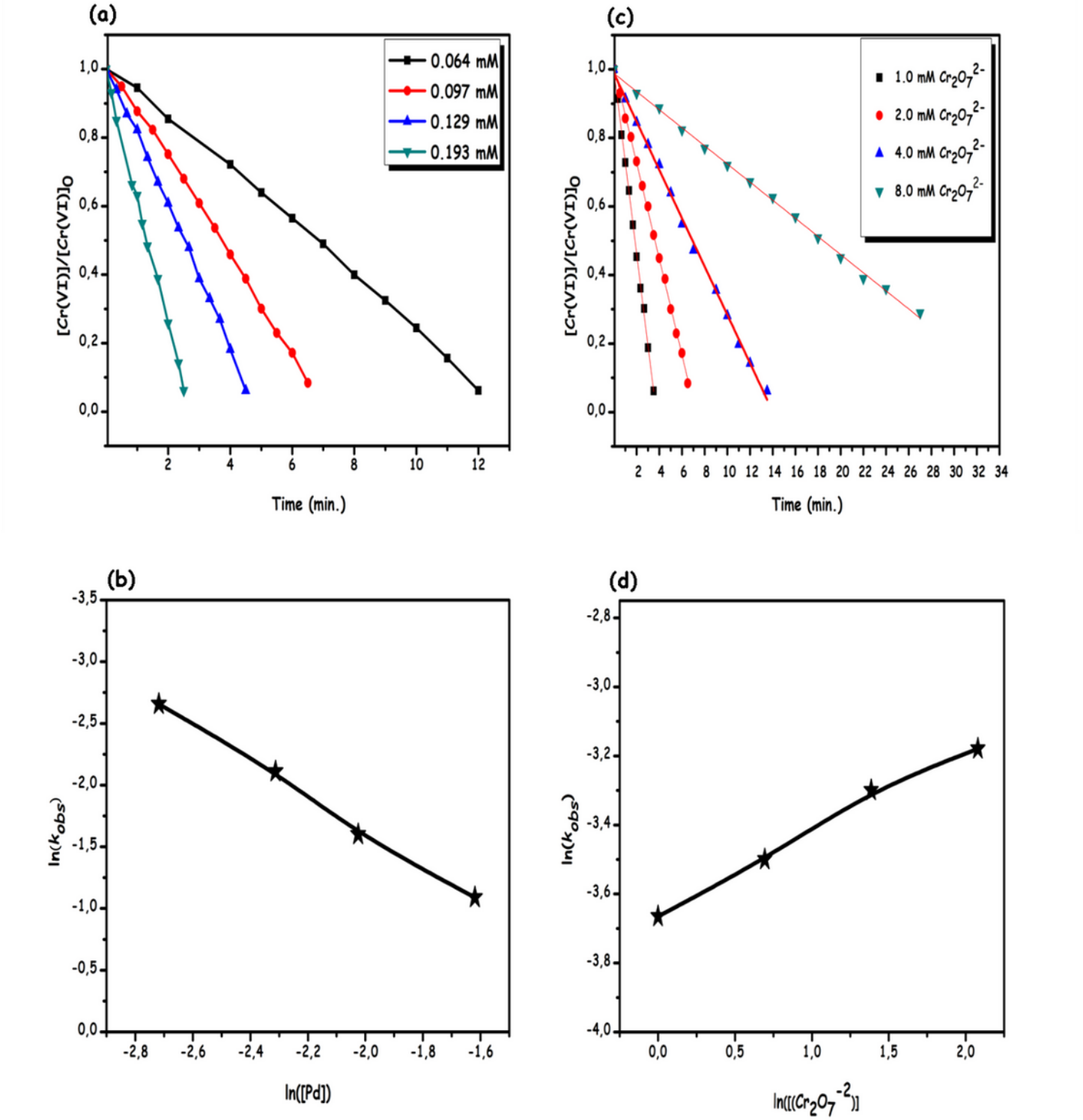

Figure 7

(a) Graph of remaining Cr(VI) ratio ([Cr(VI]/[Cr(VI)]0] against time, (b) graph of [Pd] concentration against kobs values obtained from (a) (logarithmic values of both), (c) graph of remaining Cr(VI) ratio ([Cr(VI]/[Cr(VI)]0] against time, (d) graph of [Cr2O72−] concentration against kobs values obtained from (c) (logarithmic values of both).

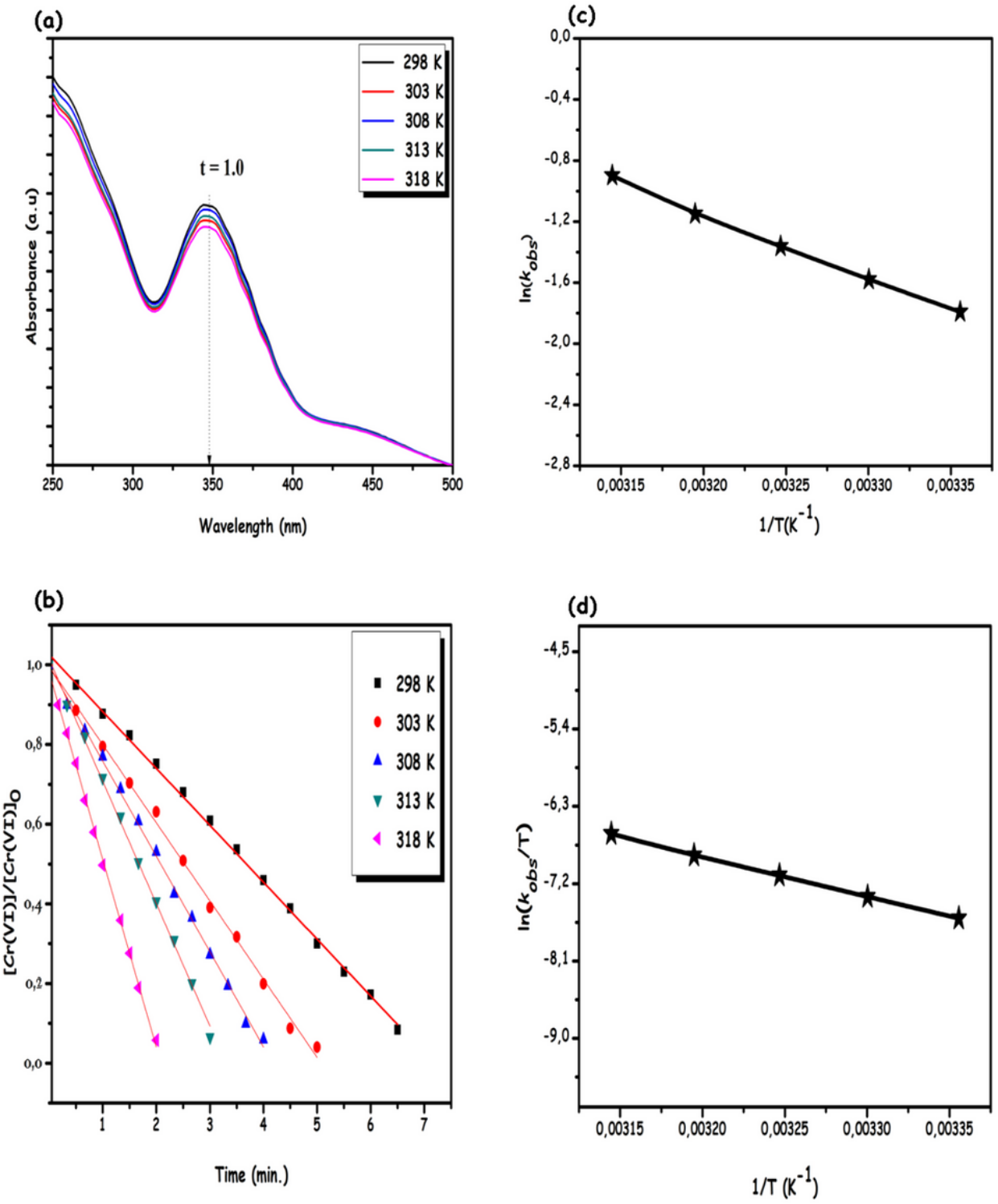

Figure 8

(a) UV-vis spectroscopy of Pd(0)@C catalyst at t = 1min., (b) graph of remaining Cr(VI) ratio ([Cr(VI]/[Cr(VI)]0]) against time, (c) plots of Arrhenius and (d) Eyring-Polonyi obtained from the data in (b).

Supplementary Files

This is a list of supplementary files associated with this preprint. Click to download.

- SupplementaryMaterial.docx